Journal of Nuclear Materials 441 (2013) 240–251

Contents lists available at SciVerse ScienceDirect

Journal of Nuclear Materials

journal homepage: www.elsevier.com/locate/jnucmat

Coupled thermochemical, isotopic evolution and heat transfer simulations in highly irradiated UO_2 nuclear fuel

M.H.A. Piro [a,*], J. Banfield [b], K.T. Clarno [c], S. Simunovic [d], T.M. Besmann [a], B.J. Lewis [e], W.T. Thompson [e]

[a] Materials Science and Technology Division, Oak Ridge National Laboratory, Oak Ridge, TN, USA
[b] Nuclear Engineering Department, University of Tennessee, Knoxville, TN, USA
[c] Reactor and Nuclear Systems Division, Oak Ridge National Laboratory, Oak Ridge, TN, USA
[d] Computer Science and Mathematics Division, Oak Ridge National Laboratory, Oak Ridge, TN, USA
[e] Department of Chemistry and Chemical Engineering, Royal Military College of Canada, Kingston, ON, Canada

ARTICLE INFO

Article history:
Received 28 January 2013
Accepted 27 May 2013
Available online 7 June 2013

ABSTRACT

Predictive capabilities for simulating irradiated nuclear fuel behavior are enhanced in the current work by coupling thermochemistry, isotopic evolution and heat transfer. Thermodynamic models that are incorporated into this framework not only predict the departure from stoichiometry of UO_2, but also consider dissolved fission and activation products in the fluorite oxide phase, noble metal inclusions, secondary oxides including uranates, zirconates, molybdates and the gas phase. Thermochemical computations utilize the spatial and temporal evolution of the fission and activation product inventory in the pellet, which is typically neglected in nuclear fuel performance simulations. Isotopic computations encompass the depletion, decay and transmutation of more than 2000 isotopes that are calculated at every point in space and time. These computations take into consideration neutron flux depression and the increased production of fissile plutonium near the fuel pellet periphery (i.e., the so-called "rim effect"). Thermochemical and isotopic predictions are in very good agreement with reported experimental measurements of highly irradiated UO_2 fuel with an average burnup of 102 GW d $t(U)^{-1}$. Simulation results demonstrate that predictions are considerably enhanced when coupling thermochemical and isotopic computations in comparison to empirical correlations.

Notice: This manuscript has been authored by UT-Battelle, LLC, under Contract No. DE-AC05-00OR22725 with the U.S. Department of Energy. The United States Government retains and the publisher, by accepting the article for publication, acknowledges that the United States Government retains a non-exclusive, paid-up, irrevocable, world-wide license to publish or reproduce the published form of this manuscript, or allow others to do so, for United States Government purposes.

© 2013 Elsevier B.V. All rights reserved.

1. Introduction

The composition of nuclear fuel materials and related thermochemical properties (such as the oxygen chemical potential and the oxygen to metal ratio) greatly influence its behavior under normal and abnormal operating conditions. For instance, the local fuel chemical composition affects thermal conductivity, solid-state diffusion, grain growth, creep and fission gas release [1]. Furthermore, the chemical behavior of the fuel surface affects clad oxidation, which can potentially compromise the structural integrity of a fuel element. Many nuclear fuel codes require a method of capturing thermochemistry, isotopic depletion, transmutation and decay as they bear on matters pertaining to fuel performance and safety, yet they generally fail to adequately consider these phenomena, if at all.

From a thermodynamic point of view, the fuel has been treated in most nuclear fuel simulations as a homogenous system comprised of the $UO_{2\pm x}$ solid solution phase (which is often assumed to be stoichiometric) while neglecting the fission and activation product inventory [3–10]. In reality, several minor phases are formed in addition to the UO_2 solid solution phase as a consequence of irradiation, including the noble-metal phases (often referred to as the "white phase"), complex oxide inclusions and gas [1]. Subsequently, the microstructure of the fuel changes in both space and time, resulting in significant changes in macroscopic material properties, such as thermal conductivity [12–14].

Thermodynamic computations of irradiated fuel are performed in the VICTORIA code; however, as Olander points out, the thermodynamic analysis in VICTORIA assumes ideal mixing behavior and lacks the fidelity to adequately represent irradiated fuel chemistry [2]. Also, thermodynamic computations performed in the Model for

* Corresponding author. Tel.: +1 613 602 7476.
E-mail addresses: markuspiro@gmail.com (M.H.A. Piro), clarnokt@ornl.gov (K.T. Clarno).

0022-3115/$ - see front matter © 2013 Elsevier B.V. All rights reserved.
http://dx.doi.org/10.1016/j.jnucmat.2013.05.060

Fission-Product Release (MFPR) code [11] consider the chemical influence from fission and activation products; however, the calculations are performed with equilibrium constants (rather than sophisticated thermodynamic models), which are based on semi-ideal chemistry models [11]. Furthermore, the oxygen chemical potential in MFPR is calculated using an empirical correlation only valid for fresh fuel [11]. Consequently, the use of equilibrium constants and empirical correlations do not convey with high fidelity the original thermodynamic analysis.

To further complicate matters, the spatial distribution of fission and activation products depends on solid-state diffusion, the irradiation history, neutron flux depression across the pellet and the phenomenon commonly referred to as the "rim-effect." The rim effect describes the increased production of fissile plutonium near the rim in high burnup fuel due to a higher probability of epithermal neutron resonance absorption by ^{238}U followed by subsequent beta decay [15]. According to Rondinella and Wiss, the local burnup in the rim region can be 2–3 times greater than the average burnup in highly irradiated fuel [16]. As a result, the concentration of fission and activation products vary considerably near the rim and can therefore significantly affect thermochemical predictions of the fuel surface, such as clad oxidation.

According to Matzke, the thickness of the rim region is typically 100–200 μm and becomes significant at burnups above 45 GW d t(U)$^{-1}$ [15,17]. Matzke further points out that this region tends to have submicrometer grains, extended defects, and a relatively high concentration of intergranular pores that exhibit a "cauliflower" structure [15,17]. As a consequence of this localized region being relatively porous (up to 30% [15]) with high local burnup, the thermal conductivity in this region is relatively low and impedes heat transfer from the fuel pellet to the clad. Therefore, temperatures in the fuel may increase with the undesired effect of higher fission gas release, which is further enhanced by a higher local porosity [15,16]. Although the rim region accounts for approximately 5% of the total volume in the fuel, this region accounts for approximately 10% of the total radioactivity [15]. Accounting for the local fission product inventory and thermochemical behavior in the rim region has significant implications for performance and safety of nuclear reactor operations [15] and is thus a major driver in this work.

Predicting phase equilibria in irradiated fuel is complicated by a continually evolving fission product inventory, solid-state diffusion of multiple chemical elements (which is not considered in the current simulation framework), and an extremely large temperature gradient. Additionally, the very large number of chemical elements and the varying abilities of fission and activation products to chemically react with oxygen further complicate thermochemical predictions. Sophisticated thermodynamic models are able to describe this complex behavior; however, an efficient and robust thermodynamic solver is required to perform equilibrium calculations. Furthermore, the solver must be capable of handling a large enough number of chemical elements to sufficiently capture the fission product inventory (>40 [18]).

The direct integration of a comprehensive thermodynamic treatment of irradiated nuclear fuel into a multi-physics nuclear fuel performance code has been a significant challenge. Furthermore, the isotopic evolution of the fuel must be computed as input to thermodynamic calculations as the fuel undergoes burnup. Also, a sophisticated simulation environment is required to couple various physical phenomena in a self-consistent manner and to exploit high performance computing resources. A unique simulation capability is presented in this paper that predicts spatially dependent thermochemical behavior of nuclear fuel throughout all stages of burnup. The simulation framework is based on the coupling of the Advanced Multi-Physics (AMP), ORIGEN-S and THERMOCHIMICA codes. A brief description of AMP, ORIGEN-S and THERMOCHIMICA are provided in Sections 2–4, respectively, and predictions of this coupled simulation of UO_2 nuclear fuel behavior are presented in Section 5. Finally, the results from this simulation framework are compared to measured fission and activation product concentrations, oxygen-to-metal ratios, and the local oxygen partial pressure on highly irradiated UO_2 fuel in Section 6.

2. The Advanced Multi-Physics (AMP) code

AMP [19,20] is an open-source, multi-physics code that has been used to simulate a wide-variety of applications, including nuclear fuel performance [21], nuclear reactor analysis [22], and energy-storage systems [23]. AMP provides a robust computational environment to couple external software packages with internal physics operators to solve complex multi-physics problems in a rigorous and efficient manner. In the current work, the AMP three-dimensional solver is capable of computing the temperature distribution within the fuel using computational meshes that were generated either internally or using external tools, such as CUBIT [24]. The extensions for nuclear fuel performance were used to provide access to validated material models for UO_2 (based on models from the nuclear fuel performance code FRAPCON [25]), as well as linkages to the ORIGEN-S [26] and THERMOCHIMICA codes.

The nuclear fuel performance extensions to AMP include a neutronics preprocessor that provides a burnup-dependent power distribution with full isotopic inventory tracking using ORIGEN-S. The spatial distribution of the energy-integrated neutron flux was normalized to ensure that the user-defined linear-heat generation rate remains consistent as the spatial distribution of the isotopic inventory changes. The default energy-integrated neutron flux shape for UO_2 in a light-water reactor makes use of azimuthally-invariant Zernike polynomials [27].

The average fuel-pin ^{238}U neutron-capture cross sections generated from the SCALE library [26] were modified radially using the TUBRNP model from the nuclear fuel performance code TRANSURANUS ([28]). The development of the TUBRNP model within TRANSURANUS has been validated with irradiated fuel measurements in a Light Water Reactor (LWR) [29]. As the fuel in the simulation is depleted with a radial neutron flux distribution and a radial variation in the ^{238}U neutron-capture cross-section (i.e., the TUBRNP model), the isotopic inventory is able to demonstrate the full "rim effect.".

3. ORIGEN-S

ORIGEN-S simulates the isotopic depletion, transmutation, and decay of the fuel. The change in the concentration of a particular nuclide is computed for a given mass of material containing a space-energy-direction averaged neutron flux with flux-weighted averaged microscopic cross sections that represent the probability of a particular nuclear reaction. The neutron flux, which is a function of space, energy, direction and time, is dependent upon nuclide concentrations; therefore, a SCALE calculation is needed to provide the requisite problem-specific nuclear data. The mathematical treatment in ORIGEN-S assumes that the space-energy-direction averaged flux and flux-weighted neutron cross sections can be considered constant over a sufficiently small time interval. ORIGEN-S tracks over 2000 isotopes, including all 423 found on the ENDF-B.VII.1 cross-section library. ORIGEN-S computes the specific power due to both fission and neutron-capture.

The SCALE code system, which includes TRITON [30], was used to provide a problem-specific ORIGEN-S cross-section data library for the average fuel-pin throughout the fuel's life cycle. The data library was generated for the specific experiment simulated in this paper, which was in a Siemens 15 × 15 Pressurized Water Reactor (PWR) fuel rod with 3.5% enriched UO_2 fuel and the irradiation

history in the TRITON simulation is made to be consistent with reported values from Walker et al. [31].

4. Thermochimica

Thermodynamic computations with appropriate models predict the equilibrium combination of phases and their compositions. In brief, the objective is to determine a unique combination of species and phases that yields the minimum value of the integral Gibbs energy of a closed isothermal-isobaric system subject to mass balance constraints and the Gibbs phase rule [32]. For the case described here, a thermodynamic system is defined as a finite volume corresponding to each finite element on a three dimensional mesh representing a nuclear fuel pellet.

While thermochemical equilibrium is not achieved instantaneously, chemical kinetics typically does not play a large part in nuclear fuel simulations. First of all, chemical equilibrium is achieved in relatively short time periods due to the high temperatures experienced in nuclear fuel where the different chemical elements arising in irradiated nuclear fuel are, by the nature of fissioning, randomly mixed [1]. Secondly, the time scales in nuclear fuel performance simulations are typically very long. For instance, the total time scale in the simulation described in this paper is nearly 10 years with a typical time increment of approximately one month. Lastly, a large portion of experimental efforts pertaining to nuclear material behavior has been concerned with thermodynamic equilibrium conditions rather than time dependent conditions.

The numerical approach to computing thermodynamic equilibria in THERMOCHIMICA is described by Piro et al. [33]. In general, THERMOCHIMICA determines which phases are stable at thermodynamic equilibrium, their molar quantities and their constituent mole fractions, the chemical potentials of the system components, and the molar heat capacity, enthalpy, entropy and Gibbs energy of a thermodynamic system. This information can be used directly as input to material property models and boundary conditions used for continuum mechanics and phase field simulations.

Thermodynamic calculations require as input temperature, hydrostatic pressure, the mass of each chemical element and a thermodynamic database. Temperature is provided by AMP, the hydrostatic pressure is currently assumed constant at 1 atm[1], and ORIGEN-S provides the atom fraction[2] of each chemical element. Finally, thermodynamic data and models, which work together to describe a real system that bears comparison to actual observations, are used as input to the solver. Currently, the RMC Fuel Thermochemical Treatment (RFTT) [18,34,35] is employed, which captures the thermochemical behavior of irradiated UO_2 fuel. This treatment has been developed using the Calphad approach [36], which includes standard molar Gibbs energy equations of the pure compounds along with models that describe the mixing of constituents in non-ideal solution phases. This treatment is based on several years of model development supported by neutron diffraction experiments on fresh fuel [37] and oxidation experiments on SIMFUEL [18].

The representation of the fluorite phase in the thermodynamic model not only considers the departure from stoichiometry of UO_2, as well as numerous dissolved fission and activation product oxides. The selection of dilute fission products dissolved in the fluorite phase in this particular thermodynamic model [18] is consistent with experimental observations from Kleykamp [38]. The thermodynamic models representing the noble metal system that are used by this treatment are documented and validated by Kaye et al. [39]. This system is comprised of the noble metals Mo, Tc, Ru, Rh and Pd, which are represented by alloy phases in the face centered cubic, body centered cubic, hexagonal closed packed and tetragonal crystal structures in addition to liquid, gas and several pure stoichiometric phases. Details of the development of specific models and the overall thermodynamic treatment are given by Thompson et al. [34] and Lewis et al. [35].

The RFTT database was originally developed for CANDU fuel [34], which experiences a much lower burnup (i.e., approximately 7.5 GW d $t(U)^{-1}$) than what is considered in the current simulation (i.e., 102 GW d $t(U)^{-1}$). The original model for the fluorite phase was intended to capture urania with the inclusion of dilute fission products [34]; however, the concentration of fission products becomes significant at high burnup. The extension of this database to very high burnup is a necessary approximation for engineering applications at the current stage of development. As thermodynamic models and THERMOCHIMICA continue to be developed in parallel, progress can be made in future efforts to better capture fuel thermochemistry.

5. Simulation details

The capabilities of this simulation framework are demonstrated through the following scenario that simulates the behavior of highly irradiated UO_2 fuel for comparison with experiments conducted by Walker et al. [31]. Comparisons of predictions from this simulation framework with respect to these experiments are given in Section 6. The initial unirradiated fuel was slightly hyperstochiometric ($UO_{2.005}$) with an enrichment of 3.5%, an outer diameter of 9.3 mm and a theoretical density of 95%. The fuel was in a commercial Siemens 15 × 15 PWR fuel assembly. The fuel was irradiated over a period of 9 power cycles that spanned approximately 3500 effective full power days with an integral burnup of 102 GW d $t(U)^{-1}$ [31]. The irradiation history applied in the simulation is made to be consistent with experimental measurements from Walker et al. [31] and is shown in Fig. 1.

Admittedly, this burnup greatly exceeds the maximum allowable burnup in a PWR in the United States (as regulated by the

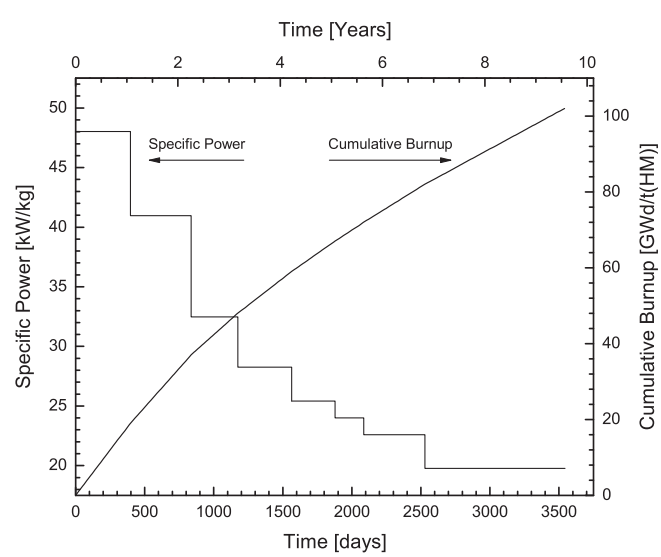

Fig. 1. The irradiation history of UO_2 fuel used in the current simulation is consistent with experiments conducted by Walker et al. [31].

[1] This is a reasonable approximation since fuel chemistry is relatively insensitive to hydrostatic pressure in comparison to temperature, the local mass fraction of each chemical element and the uncertainties associated with thermodynamic models.

[2] It is important that ORIGEN-S provides quantities in gram-atoms instead of grams because unnecessary errors would arise in converting grams to gram-atoms in THERMOCHIMICA due to the changing molar mass of each chemical element as a result of irradiation.

Nuclear Regulatory Commission (NRC)); however, this particular experiment is chosen for the current simulation framework because it is the only one known to the authors that is published in the open literature that reports both oxidation measurements and local fission product concentrations of the same sample. Matzke conducted similar experiments of fuel oxidation for lower burnup fuel at 28.9, 34.5 and 58 GW d t(U)$^{-1}$; however, neither the average nor local elemental concentrations were reported [40]. Since thermochemical computations are sensitive to the relative proportions of chemical elements, elemental concentration predictions must be validated in parallel to thermochemical predictions, as will be discussed in Section 6.

5.1. Heat transfer

The temperature distribution in a three dimensional fuel pellet is computed with AMP. A Dirichlet boundary condition (i.e., constant scalar value) is imposed on heat transfer calculations on the circumferential surface of the pellet and is assigned a value of 557.2 K. A Neumann boundary condition (i.e., no heat flux) is applied to the top and the bottom surfaces of the pellet, which is consistent with traditional one dimensional fuel performance codes. Additionally, heat transfer from pellet-to-pellet is typically much smaller than that from the pellet-to-clad. Material property models, including the specific heat capacity and thermal conductivity, are taken from FRAPCON [25]. Finally, the thermal source term due to nuclear fission makes use of the specific power of the fuel. The power profile from FRAPCON [25] is used as input to ORIGEN-S, which then recomputes the power within the same time step based on the production of fissile plutonium near the rim region. This will be further discussed in Section 5.2.

All fuel samples analyzed by Walker et al. were heated at a uniform temperature during post-irradiation examination measurements [31]. To provide a consistent basis for comparison with experiments, temperature calculations were artificially adjusted at constant temperature. Therefore, specific models that affect heat transfer in the pellet (e.g., the fuel-to-clad gap heat transfer coefficient, which depends on fission gas release) are not relevant to the current discussion for comparison purposes. However, physical models that affect heat transfer are important for adequately predicting temperature distributions of nuclear fuel under normal power conditions.

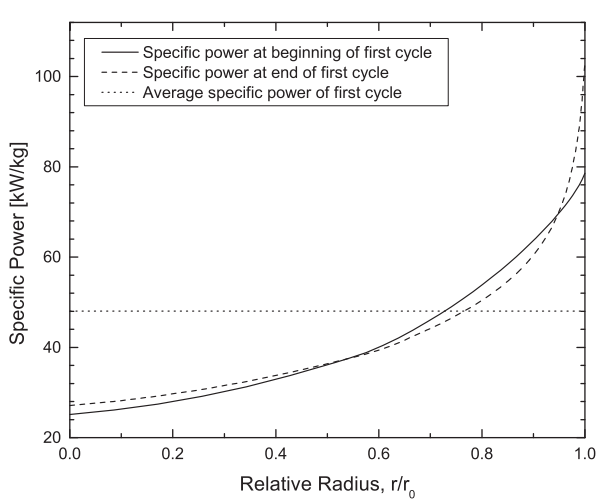

Fig. 2. The specific power profile across the pellet is shown at a burnup of 102 GW d t(U)$^{-1}$. This profile accounts for neutron flux depression across the pellet and the sharp increase in power due to the rim effect.

5.2. Isotopic depletion, decay and transmutation

Fig. 2 illustrates the spatial variation in specific power across a UO_2 fuel pellet at the beginning and the end of the first power cycle (i.e., both curves have the same average power across the pellet). The increased probability of ^{238}U capturing epithermal neutrons in the outer 5% produces an appreciable build up of fissile plutonium, which significantly increases the specific power in the outer rim, which is shown near $r/r_0 = 0.95–1.0$ in Fig. 2, where r/r_0 is the relative radius (i.e., r_0 is the outer radius of the pellet). The change in the spatial variation in specific power with average burnup affects temperature predictions (i.e., the thermal source term) in addition to the spatial variation of fission products. Thermochemical calculations are dependent on both temperature and elemental composition and are also affected by this change.

In this simulation, ORIGEN-S included more than 2000 isotopes in its internal calculations, the maximum time increment was 32 days and 10 subcycles were applied per time increment. The following chemical elements were used as input to THERMOCHIMICA: Pu, Np, U, Nd, Pr, Ce, La, Ba, Cs, Xe, I, Te, Pd, Rh, Ru, Tc, Mo, Zr, Y, Sr, Rb and O. This selection of chemical elements conforms to the content of the RFTT database [34,35]; however, a much greater number of chemical elements are stored in internal calculations within ORIGEN-S. Several of the higher actinoids, such as Am and Cm, were not used in thermochemical calculations but are important to consider in computing the isotopic evolution in the fuel and the local power density. The change in the relative proportions of chemical elements for the entire fuel pellet with burnup is illustrated in Fig. 3 using the irradiation history shown in Fig. 1.

The predicted concentration of Pu in Fig. 3 increases quite rapidly at earlier stages of burnup due to the activation of ^{238}U followed by beta decay of ^{239}U and ^{239}Np, respectively. The concentration of Pu equilibrates around 45–50 GW d t(U)$^{-1}$, which implies that the rate of production of Pu is approximately equal to the rate of fission (mostly ^{239}Pu) and capture of Pu. Since fission gas release is not simulated in the current framework, the total Xe concentration continues to grow at a high rate throughout the irradiation history.

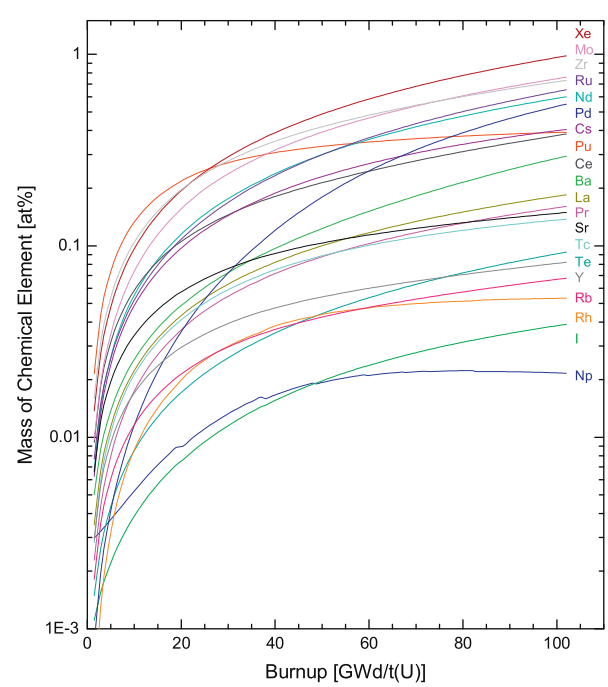

Fig. 3. The predicted evolution of the pertinent fission and activation products integrated across the pellet is illustrated.

As is demonstrated in Fig. 3, the rate that many of the fission product elements accumulate in the fuel with respect to burnup varies from one chemical element to another. Therefore, the relative proportions of chemical elements vary considerably throughout the pellet and at various stages of burnup, which have direct implications to thermochemical predictions. Perhaps the most important chemical element in Fig. 3 is Pu since the fission of ^{239}Pu contributes significantly to the specific power in the fuel, particularly in the rim region. The concentration curve for Np has several minor kinks that correspond to changes in the average linear power for the various fuel cycles (refer to Fig. 1). The predicted concentration of Np is sensitive to changes in the power since both ^{239}U and ^{239}Np have relatively short half-lives.

Although the atom fraction of fission and activation product elements are 2–4 orders of magnitude less than that of uranium and oxygen, their presence in the fuel can have a profound effect on numerous aspects of fuel behavior. For instance, many fission and activation products with very low concentrations may have significant radiological consequences. Additionally, fuel chemistry is dependent on the proportions of the elements with widely different propensities to combine with oxygen. Thus, the oxygen chemical potential can be very sensitive to compositional changes associated with burnup.

5.3. Irradiated fuel chemistry

Temperature predictions from AMP and the fission product inventory from ORIGEN-S are used directly as input to THERMOCHIMICA at every finite element and for each time increment. The selection of chemical elements considered in the simulation is consistent with the RFTT [34,35], which includes several chemical elements that were not measured by some experiments. Many of these elements were intentionally included in the simulation because they contribute appreciably to the formation of various phases. In particular, the elements Pd, Rh, Ru, and Tc (which were not measured by Electron Probe Microanalysis (EPMA) by Walker et al. [31]) are important to consider in the formation of several of the noble metal phases.

This computational framework provides a unique capability for computing the spatial variation of phases across the pellet with burnup. Fig. 4 shows the change in all phases in the radial direction at a burnup of 102 GW d t(U)$^{-1}$. As is to be expected, the fluorite oxide is the dominant phase and several additional minor phases are predicted to be stable, including noble metal inclusions in the face centered cubic and hexagonal closed packed crystal structures,

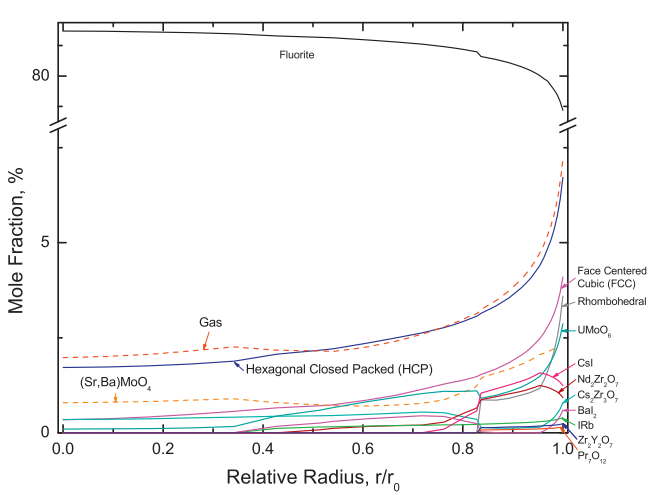

Fig. 4. The predicted distribution of phases across the pellet is shown for an average pellet burnup of 102 GW d t(U)$^{-1}$.

and other oxides, such as molybdates, uranates and zirconates. The primary metallic inclusion phase predicted in this simulation is in the hexagonal closed packed crystal structure (as shown in Fig. 4), which is consistent with experimental observations by Kleykamp [41,42].

Additional oxide phases that are insoluble in the fluorite oxide matrix are also formed, which are often referred to as the "gray phase". The SrO and BaO oxides have limited solubility in the fluorite phase due to the relatively large radii of the Ba^{2+} and Sr^{2+} cations [1], and chemically associate with other elements to form additional phases. These solid oxides are generally represented by $(Ba,Sr,Rb_2,Cs_2)(U,Zr,Mo)\,O_{3_{(s)}}$ and have a perovskite crystal structure [1,34].

A few additional phases are predicted to form in the fuel, including $UMoO_{6_{(s)}}$, $Cs_2Zr_3O_{7_{(s)}}$, and gas [34]. Several of the fission products with very low solubility in the fluorite phase form stable gaseous species in the form of bubbles that accumulate in the grains and on the grain boundaries and eventually migrate to the fuel-to-clad gap. Although $Xe_{(g)}$ and $Kr_{(g)}$ are generally the dominant gaseous species (since they are chemically inert and have high fission yields), several other fission product elements contribute appreciably to the gas phase in addition to other phases. For instance, Cs and Rb are expected to be stable in the gaseous phase in addition to other solid phases, in particular the perovskite, fluorite solid oxides and iodides [34]. The mechanism of modeling fission gas release has not been included in the current simulation framework and is expected to affect both predicted elemental distributions of the fission product elements and thermochemical predictions. Thus, these calculations may be used in future simulation efforts in performing higher fidelity predictions of fission gas retention.

The relative proportion of the fluorite phase decreases from the center of the pellet to the fuel surface, while the concentration of minor phases generally increases. This trend is consistent with the spatial variation of burnup. The slight kink in the phase distribution in Fig. 4 near $r/r_0 = 0.83$ is due to the introduction of the rhombohedral phase to the system. The rhombohedral phase is represented in the current treatment as an ideal solid solution of $UO_3(Ln_2O_3)_3$, where Ln represents the lanthanoid elements Ce, Nd and La [34]. The formation of the rhombohedral phase in this region is simply due to the unique combination of chemical elements that is thermodynamically favorable for it to be stable.

In addition to predicting the combination of phases and their quantities within the pellet, THERMOCHIMICA provides many useful thermodynamic properties. For instance, the local oxygen chemical potential is generally considered to be one of the most important chemical properties in the fuel because it affects many diffusion controlled processes and oxidation of the inner surface of the clad. Fig. 5 illustrates the predicted spatial variation of the partial pressure of diatomic oxygen gas (graphically represented as $\Delta\bar{g}_{O_{2(g)}} = RT\ln p_{O_{2(g)}}$) in equilibrium with the fuel at power. The convex behavior in the oxygen partial pressure profile is due to competing effects of temperature and local burnup, which will be discussed in greater detail in Section 7.

6. Comparison of predictions with experiment

The current discussion will provide details on independently comparing isotopic evolution and thermochemical predictions with experiments followed by an integrated comparison study with respect to post-irradiation examination measurements [31]. The TRITON depletion capability within SCALE has been validated for many fuel and reactor configurations with many data libraries. The current validation evaluation is provided by Ilas et al. [44] using ENDF/B-VII cross-sections and version 6.1 of SCALE. The

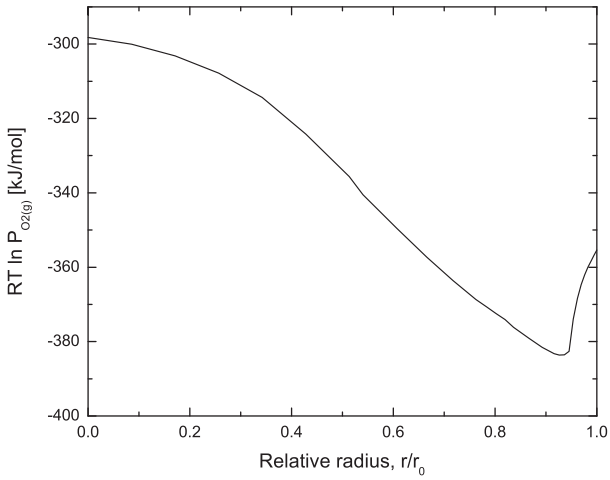

Fig. 5. The spatial variation in the predicted oxygen partial pressure of in-reactor fuel is convex, which corresponds to competing effects from temperature and local burnup variations along the radial direction.

isotopic validation study includes comparisons with actinoids and fission products within an entire fuel rod. The UO_2 validation suite includes fuel with a discharge burnup of 70 GW d t(U)$^{-1}$ from the Gosgen reactor and, with an ENDF/B-V data library, up to 78 GW d t(U)$^{-1}$ from the Vandellos II PWR library [45]. However, there has not been any validation of the radial variation of isotopes within a single fuel pellet using SCALE.

The development of the RFTT involves numerous thermodynamic models corresponding to different phases that may be produced in irradiated UO_2 nuclear fuel. Individual models pertinent to various binary and ternary thermodynamic systems have been validated independently in addition to integral validation studies [18]. The cornerstone of the treatment rests on the uranium–oxygen binary system, in particular the non-stoichiometric $UO_{2\pm x}$ solid solution phase. As demonstrated by Thompson et al. [34] and Lewis et al. [35], the relationship between temperature, composition and the predicted partial pressure of diatomic oxygen gas agree well with the work of Lindemer and Besmann [46] and many other experimental studies for fresh fuel [47]. Additionally, binary and ternary systems belonging to the noble metals (Mo, Tc, Ru, Rh and Pd) that are incorporated in this treatment have been validated by Kaye et al. [39]. Finally, integrated validation studies of the full thermochemical treatment have been performed by Corcoran et al. with respect to SIMFUEL oxidation experiments at the Chalk River Laboratory [18].

Measurements of the local fission product inventory, oxygen-to-metal ratio and oxygen partial pressure from Walker et al. [31] are used for comparison purposes in this simulation framework. The fuel sample prepared by Walker et al. was a 1 mm thick disk cut from a pellet located on the upper end of the fuel stack [31]. Several measurements were made along the radial direction of this sample at $r/r_0 = 0.10$, $r/r_0 = 0.50$, $r/r_0 = 0.80$, and $r/r_0 = 0.975$. Measurements made at $r/r_0 = 0.975$ were intended to capture the rim effect, which corresponds to a depth of 116 μm from the fuel surface. This depth is consistent with Matzke's observations of the thickness of the rim region [15]. The ensuing discussion exclude measurements taken at $r/r_0 = 0.10$ because Walker et al. report that measurements of the electromotive force (EMF) were not reproducible in this region resulting in very large errors [31].

6.1. Integral fuel elemental composition

The integral elemental composition of the fuel was measured using inductively coupled plasma mass spectrometry (ICP-MS) [31] and is compared to predicted values from this work in Fig. 6. For the most part, the predicted concentrations of individual fission and activation product elements agree well with measured values within the reported experimental error of 10%. Walker et al. report that the concentrations of the noble metals Mo, Tc, Ru, Rh and Pd are not representative of the true values after irradiation because they have remained as residue after dissolution of the fuel [31]. The error bars for these particular elements are intentionally excluded from Fig. 6 for this reason. Several pertinent chemical elements – specifically, O, Xe and Kr – are not shown in Fig. 6 because they cannot be measured by ICP-MS [31].

6.2. Local fuel elemental composition

Local concentrations of the fission and activation products were measured by EPMA [31] and are compared to predicted values in Figs. 7–9 at $r/r_0 = 0.50$, 0.80 and 0.975, respectively. Several chemical elements that were not measured – specifically, Tc, Ru, Rh, Pd, Te and I – are included in the simulation because they contribute to the formation of many pertinent phases. For the most part, the predicted local concentration of most elements are in good agreement with EPMA measurements.

6.3. Radial distribution of plutonium

As reported by Walker et al., the cumulative burnup after the third irradiation cycle resulted primarily from the fission of ^{239}Pu rather than ^{235}U [31]. Furthermore, the total amount of Pu that was created during irradiation was estimated to be approximately four times greater than what remained at the end of irradiation [31].

Fig. 10 compares the predicted distribution of Pu to EPMA measurements by Walker et al. Clearly, the Pu concentration that is shown in Fig. 10 represents the quantity that remains at the end of irradiation. As is to be expected, the Pu concentration increases gradually from the center of the pellet through most of the bulk material and increases sharply near the rim, following a similar trend to the power profile in Fig. 2. Arrows are superimposed on Fig. 10 to locate the four radial positions where the local fission product inventory and oxygen partial pressure measurements were made.

Unfortunately, experimental errors were not reported for any of the EPMA measurements; however, the errors in ICP-MS measurements (as shown in Fig. 6) for the average concentrations of all elements were reported to be 10%. Theoretically, the integral Pu concentration using EPMA measurements (i.e., Fig. 10) should be consistent with the reported Pu concentration using ICP-MS measurements (i.e., Fig. 6). Performing numerical integration using the Trapezoidal rule in cylindrical co-ordinates[3] on EPMA measurements from Fig. 10 reveals that the integral Pu concentration is 29% higher than the reported value from ICP-MS measurements.

It is believed that errors associated with integral ICP-MS measurements are lower than the EPMA measurements because EPMA measurements were only performed in one radial direction and it may be possible that the Pu content varied both radially and azimuthally. Since ICP-MS measurements were made on the bulk material, any variations in the azimuthal direction will therefore be accounted for by this technique. Also, EPMA measurements of the Pu concentration relied on a correction for X-ray line interference between U and Pu [31], which further contributes to the uncertainty. An additional plot is included in Fig. 10 that

[3] The concentration, c, of a particular chemical element integrated across the pellet makes use of the Trapezoidal rule in cylindrical co-ordinates: $c = \frac{1}{r_0^2}\sum_{i=1}^{N}(r_{i+1} - r_i)(r_{i+1}c(r_{i+1}) + r_i c(r_i))$, where r_i is the relative radius associated with point r_i, r_0 is the outer radius of the pellet, $c(r_i)$ is the concentration at i and N is the number of integration points.

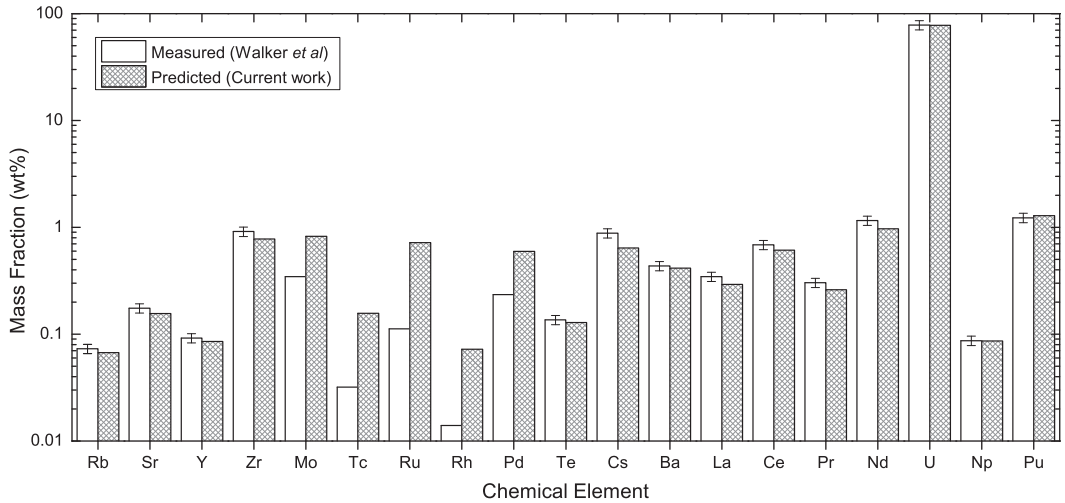

Fig. 6. The predicted average fission product inventory in the fuel is compared to ICP-MS measurements from Walker et al. [31] at 102 GW d t(U)$^{-1}$.

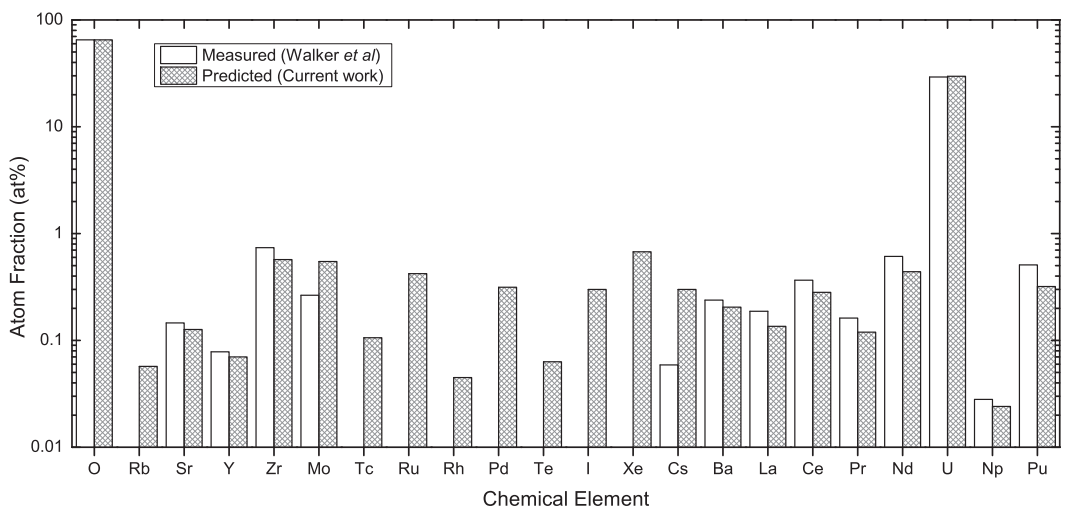

Fig. 7. The predicted local fission product inventory from this work is compared to EPMA measurements from Walker et al. [31] at $r/r_0 = 0.50$.

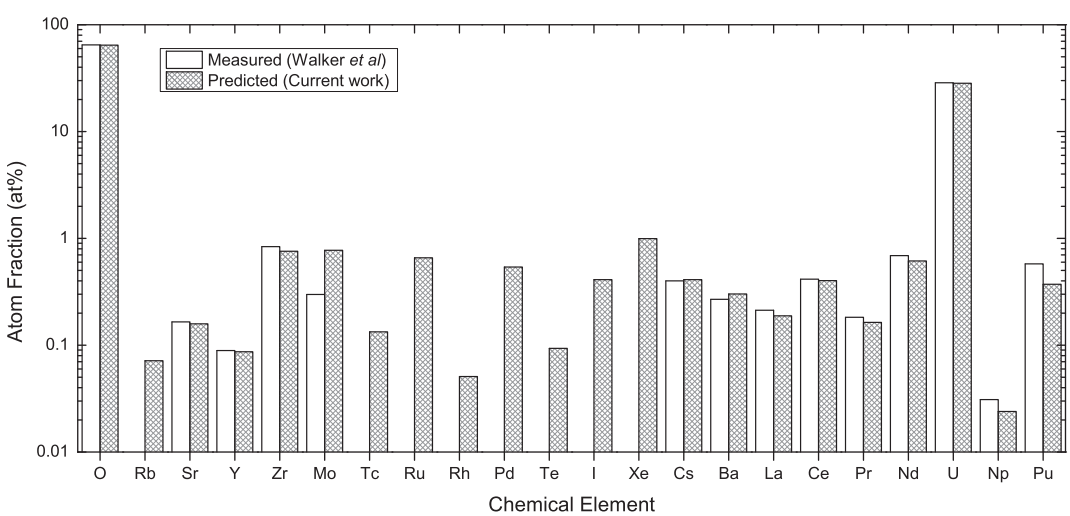

Fig. 8. The predicted local fission product inventory from this work is compared to EPMA measurements from Walker et al. [31] at $r/r_0 = 0.80$.

normalizes the measured EPMA data points to yield a consistent integral value with the ICP-MS measurements in order to provide a more consistent basis for comparison. One should keep in mind that the foregoing issues affect comparisons made between predicted and measured values by EPMA reported in Figs. 7–9 that bring the predicted and measured quantities closer together.

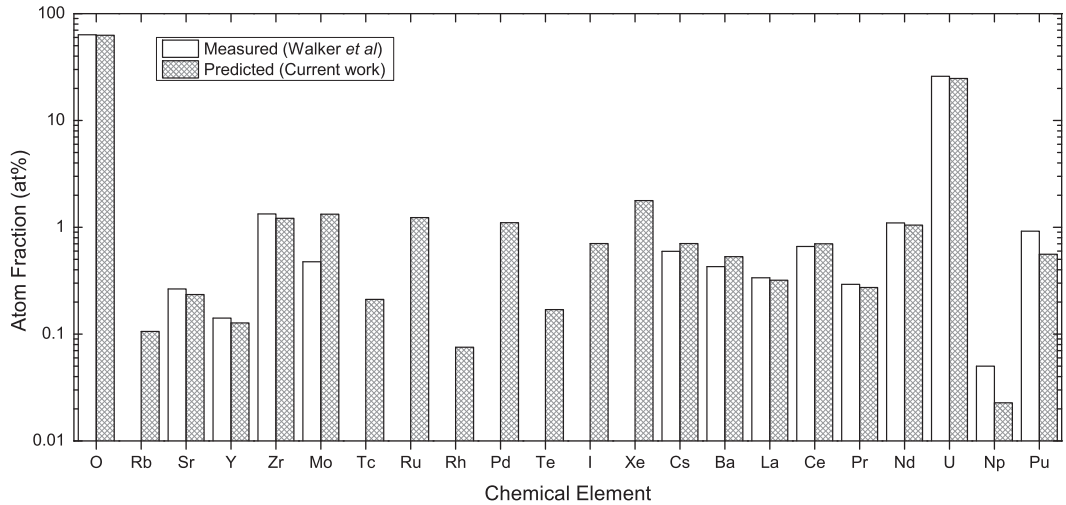

Fig. 9. The predicted local fission product inventory from this work is compared to EPMA measurements from Walker et al. [31] at $r/r_0 = 0.975$.

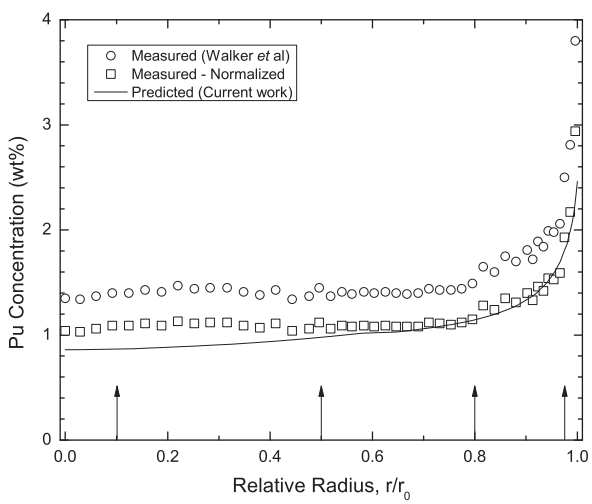

Fig. 10. The predicted radial distribution of plutonium is compared to EPMA measurements by Walker et al. [31]. A normalized data-set is included that yields a consistent integral Pu concentration with ICP-MS measurements.

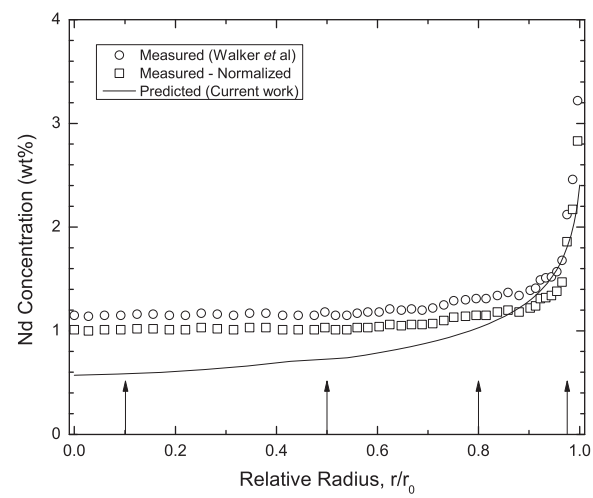

Fig. 11. The predicted radial distribution of neodymium is compared to measurements by Walker et al. [31]. A normalized data-set is included that yields a consistent integral Nd concentration with ICP-MS measurements.

6.4. Radial distribution of neodymium

Fig. 11 compares the radial distribution of Nd predicted in the current work to EPMA measurements from Walker et al [31]. Since Nd atoms are immobile in the fluorite crystal structure [31], the local concentration of Nd was used by Walker et al. to estimate the local burnup in the fuel. The local burnup at four radial positions were calculated by Walker et al. on the premise that the integral burnup across the pellet is equal to 102 GW d $t(U)^{-1}$ and is linearly dependent on the Nd concentration.

While the average linear power and burnup can be relatively easily measured, the local burnup in the fuel pellet varies due to neutron flux depression toward the centerline of the pellet and the sharp increase in the rim region. The local burnup at radial positions $r/r_0 = 0.10$, 0.50, 0.8 and 0.975 that have been experimentally inferred by Walker et al. are compared to predicted values in the current work in Fig. 12. One must keep in mind that the reported local burnup that was inferred from measured Nd concentrations does not have direct consequence to predicted values in the current simulation framework. The predicted local burnup in the simulation is not based on local Nd concentrations, but rather

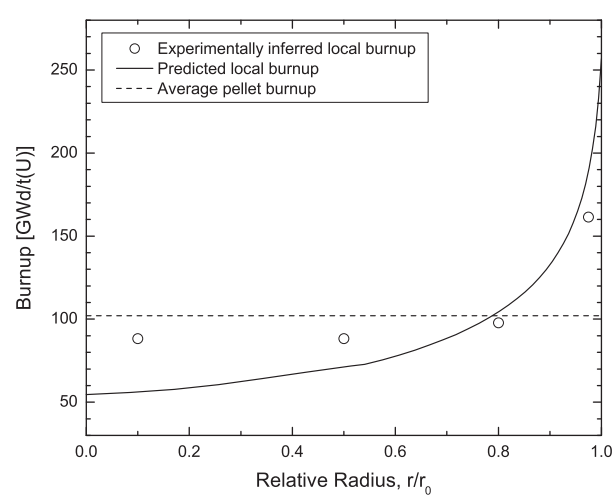

Fig. 12. The predicted variation in local burnup across the pellet is shown at the end of irradiation and is compared to experimentally inferred values [31]. The local burnup is computed by integration of the local specific power with time and does not make use of the local Nd concentration.

the local burnup at any point in space is calculated by integration of the specific power with time.

6.5. Oxygen to metal ratio

The proportion of oxygen to metal atoms (i.e., the O/M ratio) in the bulk material necessarily decreases as a result of fission. However, the O/M ratio in the fluorite phase – which differs from the bulk multi-phase system – is difficult to measure and predict because many non-metallic elements do not form oxides nor are soluble in the fluorite phase. To avoid confusion, the following text will use the symbol $(O/M)_b$ to represent O/M in the bulk material and $(O/M)_f$ will correspond to the fluorite crystal structure. Walker et al. [31] report that $(O/M)_f$ decreases with burnup from 2.005 to 1.973, which was inferred by EPMA measurements at the four radial positions [31].

Fig. 13 compares the predicted $(O/M)_f$ with reported values from Walker et al. at 102 GW d $t(U)^{-1}$, who provide two data-sets for the experimentally inferred $(O/M)_f$. Since $(O/M)_f$ cannot be measured directly, it was inferred by local EPMA measurements along the radial direction and Walker et al. assumed that a particular chemical element was stable in either the fluorite phase or a secondary oxide phase. The first experimentally inferred data-set in Fig. 13 is based on the assumption that Mo is stable as an oxide and the second assumes that it is stable as a metal. Walker et al. report that the main source of error in reported $(O/M)_f$ values is due to the uncertainty about the chemical state of Zr, Mo and Cs [31].

The thermodynamic treatment in this simulation does not make any a priori assumptions as to which phases are stable and many chemical elements may contribute to multiple phases. For instance, Mo is predicted to be soluble in the fluorite phase, perovskite phase, $UMoO_6$, face centered cubic and hexagonal closed packed metallic phases. Predicted values of $(O/M)_f$ are generally in good agreement with experimentally inferred values. The short plateaus and changes in the predicted $(O/M)_f$ profile near the rim are due to changes in the predicted phase assemblage, as shown in Fig. 4. Generally, $(O/M)_f$ is predicted to be around 1.99 throughout the fuel at an integral burnup of 102 GW d $t(U)^{-1}$, which is within the uncertainty of experimentally inferred values.

6.6. Oxygen partial pressure

The oxygen chemical potential of *unirradiated* UO_2 fuel is well understood over a wide range of temperature and composition [46]. Conversely, the oxygen chemical potential of *irradiated* UO_2 fuel is not well understood and difficult to measure over the entire range of operating conditions [31,40]. Thermodynamic models provide a basis for predicting the oxygen chemical potential of irradiated fuel, which are also dependent on the predicted fission product inventory.

Oxygen partial pressure measurements were made by Walker et al. using a miniature solid-state galvanic cell at various locations in the fuel [31]. Fig. 14 compares the predicted oxygen partial pressure (graphically represented as $\Delta\bar{g}_{O_{2(g)}} = RT\ln p_{O_{2(g)}}$) with measured values from Walker et al. for three radial positions at $r/r_0 = 0.50$, $r/r_0 = 0.80$ and $r/r_0 = 0.975$. Again, a comparison of $\Delta\bar{g}_{O_{2(g)}}$ is not made at $r/r_0 = 0.10$ due to the very large errors reported for those measurements. The changes in curvature in $\Delta\bar{g}_{O_{2(g)}}$ predictions are a result of minor phase transitions, similar to what is shown in Fig. 4.

The uncertainties and errors concerning EPMA measurements shown in Fig. 14 involve contributions from multiple sources. For instance, fluctuations in voltmeter readings contributed approximately 1–2% to the EMF uncertainty [48]. Additional sources include sampling uncertainty, uncertainty of the radial position, and errors resulting from possible alteration of the oxidation state of the sample during storage and handling. Taking into account all contributing factors, a conservative estimate of the overall measurement uncertainty of $\Delta\bar{g}_{O_{2(g)}}$ in Fig. 14, with exception of measurements at $r/r_0 = 0.10$, is approximately 10% [48].

The variation in $\Delta\bar{g}_{O_{2(g)}}$ with respect to radial position is shown in Fig. 15 at 750 °C and 1000 °C and is compared to experimental measurements. As a general trend, values for $\Delta\bar{g}_{O_{2(g)}}$ increase from the center of the fuel to the fuel surface at both temperatures with a steeper trend near the rim region. Since the elemental concentration does not change significantly from the center of the pellet to approximately $r/r_0 = 0.50$, values for $\Delta\bar{g}_{O_{2(g)}}$ are not expected to change significantly at constant temperature in this region. Since the error in EPMA measurements at $r/r_0 = 0.10$ is very high, the authors expect that the true value of $\Delta\bar{g}_{O_{2(g)}}$ at this point is much higher than the reported value.

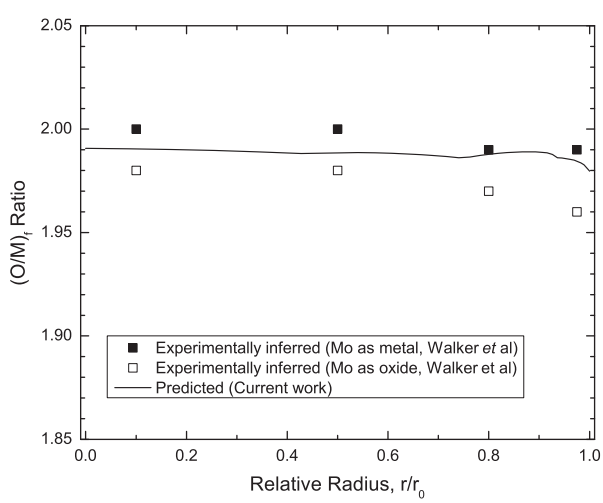

Fig. 13. The predicted radial distribution of $(O/M)_f$ is compared to experimentally inferred values by Walker et al. [31]. Note that $(O/M)_f$ cannot be measured directly, but is inferred from other measurements.

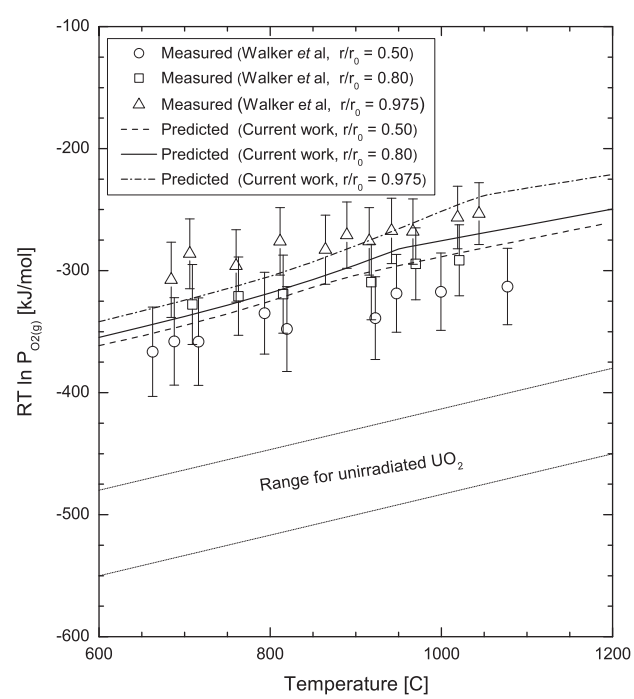

Fig. 14. The predicted oxygen partial pressure is compared to experimental measurements by Walker et al. [31].

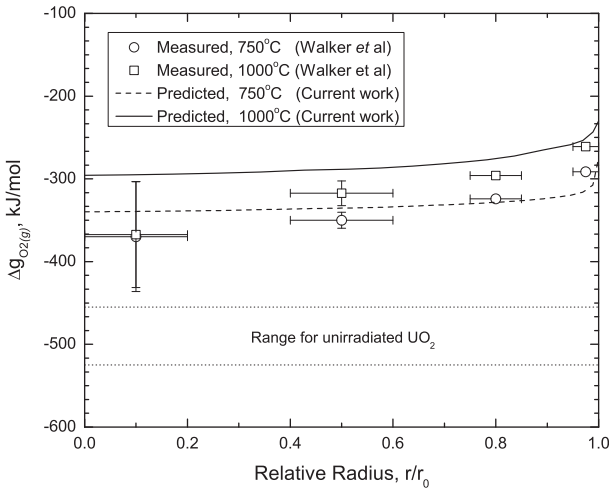

Fig. 15. The predicted oxygen partial pressure is compared to experimental measurements by Walker et al. [31] at various radial positions.

7. Discussion

Traditionally, isotopic and thermochemical computations are performed independently and are applied to point calculations. That is to say that the isotopic inventory is traditionally computed as an averaged quantity across the pellet (i.e., spatial variations are not considered) using the average power of the pellet, which is then provided as input to thermochemical computations for one fuel composition (i.e., one point in time/burnup) and one temperature. Furthermore, heat transfer, isotopic and thermochemical computations were not directly coupled. As has been demonstrated in the previous section, the fidelity of the simulation framework presented in this paper has benefited tremendously from computing the spatial and temporal variation in isotopic depletion, decay and transmutation coupled to thermochemical computations.

Predictions of the elemental concentrations of fission and activation products in the fuel are generally in good agreement with experimental measurements, especially at high burnup. Typically, the uncertainties in isotopic evolution predictions become more pronounced at higher levels of burnup. To minimize the uncertainty in these predictions, efforts were made to most closely represent experimental conditions within the simulation framework. For instance, TRITON was used to generate a unique ORIGEN-S cross-section library for this specific experiment. This TRITON simulation incorporated the specific geometry of the assembly, geometry of the fuel pellet, enrichment, and irradiation history in the reactor (as shown in Fig. 1).

The ORIGEN-S code was integrated within the AMP code and the TUBRNP model was used to account for the spatial variation of ^{238}U neutron capture cross-sections. This has demonstrated that the use of the TUBRNP model is sufficient to accurately predict the radial variation of Pu at a very high burnup. The pellet-averaged inventory of a wide variety of chemical elements at discharge was shown to have excellent agreement with experimental data. However, the results for Nd demonstrate that, though this approach was sufficient for capturing the pellet-averaged quantities of fission products, there are limitations in its use in modeling all elements. This is potentially a limitation in the accuracy of SCALE at such a high burnup, but is more likely associated with the use of TRITON and the specific power profile provided as input.

The results in Figs. 6–9 demonstrate that the predicted Nd concentrations are in relatively good agreement with experimental measurements, despite being well beyond the validated basis of SCALE. However, Fig. 11 demonstrates appreciable differences in the spatial variation of measured Nd concentrations, which is likely attributed to the manner in which SCALE was used. A single ORIGEN-S data library was produced from a SCALE depletion calculation using TRITON and used in this work to provide the spatially-averaged cross sections and the TUBRNP shape was used to approximate the effects of all radial variation in the cross sections.

For the most part, the predicted average concentrations of most chemical elements in the fuel pellet are in good agreement with ICP-MS measurements. The spatial distribution of these chemical elements, however, demonstrates greater differences between simulations and experiments. As has been demonstrated in Section 6.3, experimental errors associated with EPMA measurements may have contributed to this discrepancy. Normalizing EPMA measurements of spatially varying elemental concentrations with respect to averaged ICP-MS measurements yield consistent data-sets, and predictions are more in line with measurements. Another contributor to this discrepancy is the lack of fission gas release models in the simulation. The transport of fission gases, in particular Xe and Cs, is expected to affect isotopic predictions. For instance, the concentration of Cs is over-predicted in Sections 6.1 and 6.2, but in reality some Cs is chemically stable as a gas and over a sufficient amount of time this gas migrates to the fuel-to-clad gap.

Predicted values of various thermochemical properties are in good agreement with measurements performed by Walker et al. within the reported experimental errors. The general trend of increasing $\Delta\bar{g}_{O_{2(g)}}$ with respect to temperature is consistent among all measurements and predictions in Fig. 14. Also, both experiments and simulations show an increase in $\Delta\bar{g}_{O_{2(g)}}$ with burnup. A range of experimentally measured values of $\Delta\bar{g}_{O_{2(g)}}$ for *unirradiated* fuel have been included in Figs. 14 and 15 to demonstrate the importance of incorporating fission and activation products in the thermochemical analysis.

For the case of in-reactor fuel at power, the temperature profile decreases radially from the center of the pellet to the fuel surface, whereas the local burnup increases steadily through the bulk material and increases exponentially in the rim region. Thus, the relative contributions from both of these mechanisms to computed values of $\Delta\bar{g}_{O_{2(g)}}$ vary spatially and temporally. At early stages of burnup, the predicted $\Delta\bar{g}_{O_{2(g)}}$ profile is most strongly dependent on temperature, while contributions from fission and activation products, in particular in the rim region, become significant at high levels of burnup. As a result, the predicted $\Delta\bar{g}_{O_{2(g)}}$ profile at high burnup contains a minima (as shown in Fig. 5) that corresponds to competing effects from temperature and local burnup. The actual radial variation of $\Delta\bar{g}_{O_{2(g)}}$ of in-reactor fuel at power is not expected to exhibit this trend because the gradient in the oxygen chemical potential drives Fickian diffusion of oxygen ions, which would drive oxygen diffusion to the surface resulting in chemical interaction with the clad. Thus, this mechanism would most likely result in a smoother distribution in $\Delta\bar{g}_{O_{2(g)}}$ as a result of oxygen redistribution. Clearly, a comprehensive analysis including simulating oxygen diffusion in irradiated fuel should capture these competing mechanisms in predicting $\Delta\bar{g}_{O_{2(g)}}$.

A significant advantage of the current work is that the fuel is not approximated as a homogenous system solely comprised of the $UO_{2\pm x}$ fluorite phase, rather minor phases are predicted to co-exist with the fluorite phase. Many chemical elements may simultaneously contribute to multiple phases, which have direct implications in predicting $(O/M)_f$. For instance, Mo is predicted to be stable in the fluorite phase in addition to metallic hexagonal closed-packed, face centered cubic and several other minor phases. Walker et al. [31] have demonstrated the sensitivity of calculating $(O/M)_f$ when assuming that Mo is stable as either an oxide or a metal. This assumption is unnecessary in the current simulation framework because Mo is permitted to be stable in multiple phases simultaneously.

7.1. Future efforts and recommendations

There are several areas where the neutronics resolution could be improved, such as including a temperature variation in the fuel in the TRITON calculation and generating many ORIGEN-S data libraries that represent radial rings within the fuel. If the spatial variation of temperature were incorporated in the SCALE calculation and an ORIGEN-S data library were created for many individual annuli, then the TUBRNP model would not be required and the fission product elements would be predicted with better accuracy within SCALE. Another option would be to couple a full neutronics code, rather than just ORIGEN-S, with THERMOCHIMICA to replace the two-step approach used here.

Recent advances in TRANSURANUS [43] have improved isotopic evolution calculations to include U, Np, Pu, Am, Cm and He as input to fuel performance simulations [49]. The predicted radial distributions of these chemical elements from TRANSURANUS are in excellent agreement with EPMA measurements. The radial neutron flux model, TUBRNP, that is used in TRANSURANUS was most likely developed with respect to these types of measurements. The simulation framework described in the current paper could benefit in future efforts by replacing the neutron flux model (that was originally intended as input to thermal boundary conditions) with a similar model as in TRANSURANUS as input to ORIGEN-S. The authors expect that this would better reproduce Nd concentration profiles while also addressing the under-prediction of $\Delta\bar{g}_{O_{2(g)}}$ near the pellet rim and the over-prediction near the center. An advantage of the current work is that a full compliment of more than 2000 isotopes are currently considered, which allows for convenient predictions of virtually every fission and activation product element.

Thermochemical predictions, in particular $\Delta\bar{g}_{O_{2(g)}}$, are dependent on a number of factors including the thermodynamic models that are employed, elemental concentrations of the fission products from ORIGEN-S, the spatial variation of fission products (resulting primarily from the power profile shown in Fig. 2), and mass transport of various chemical elements across the pellet. The greatest contributor to differences between thermochemical predictions and what is actually experienced in the fuel is believed to be due to the lack of mass diffusion calculations coupled with thermochemical and isotopic predictions.

The convex trend in $\Delta\bar{g}_{O_{2(g)}}$ that is predicted in the current simulation framework in Fig. 5 for in-reactor fuel at power is expected to be significant in predicting oxygen diffusion. As demonstrated by Mihaila et al. [9] and Stan [12] in simulating coupled heat transfer and oxygen diffusion of fresh UO_{2+x} fuel, oxygen is redistributed from regions of low temperature to regions of high temperature in the fuel. However, the simulation from Mihaila et al. and Stan did not predict the local distribution of fission products or the resulting effect of irradiation on thermochemistry [9,12]. Since oxygen diffusion is driven by the gradient in the oxygen chemical potential (which could be provided by THERMOCHIMICA), oxygen is expected to be driven from the bulk material to the center of the pellet due primarily to thermal contributions to $\Delta\bar{g}_{O_{2(g)}}$, whereas oxygen is expected to be driven to the fuel surface near the rim region due to the change in curvature of $\Delta\bar{g}_{O_{2(g)}}$. Simulating oxygen transport and thermochemistry is especially important to consider near the fuel surface where oxygen may be gettered by the Zircaloy cladding. As reported by Walker et al., approximately one quarter of the "free oxygen" in their experiments was gettered by the clad [31]. These observations are also consistent with fuel oxidation experiments performed by Kleykamp [41]. Thus, incorporating oxygen diffusion in the current framework is expected to reduce $(O/M)_f$ and $\Delta\bar{g}_{O_{2(g)}}$ near the pellet periphery.

Understanding the mechanisms that govern mass transport is important in predicting fuel behavior under normal and abnormal operating conditions. For instance, oxygen can be redistributed in the fuel resulting in significant changes to local elemental composition. Since the thermal conductivity of the fuel is dependent on the local proportions of atoms, oxygen redistribution can have a significant effect on temperature predictions. As has been demonstrated by Mihaila et al., the inclusion of non-stoichiometry (assuming fresh fuel) in coupled heat and mass transfer simulations of $UO_{2\pm x}$ fuel can change centerline temperature predictions by more than 100 K under normal operating conditions [9]. According to Stan [12], a particular area that requires further research must address the role of diffusion at the grain boundary, which is further complicated when heterogeneity is accounted for in the fuel.

An advantage of the current simulation framework is that incorporation of chemical effects on the Zircaloy cladding in future efforts is relatively straightforward and simply requires appropriate thermodynamic models to be included in the database. For example, an extension of this framework could be used to investigate such phenomena as the accumulation of volatile fission product gases in the gap, particularly iodine and cesium, which may chemically react with the bare zirconium alloy cladding exposed by virtue of cracks/fissures in the normally protective ZrO_2 passive coating. This is where Iodine-induced Stress Corrosion Cracking (I-SCC) can arguably initiate [50]. Once the crack is initiated, it can propagate through intragranular and transgranular cracking modes [35]. The current framework can thus be used to provide source terms for models describing gap and clad behavior.

In addition to predicting the combination of phases and their quantities within the pellet, THERMOCHIMICA provides many useful thermodynamic properties that may be used as input to other transport phenomena. For instance, several system variables can be computed in the fuel, such as the local molar heat capacity, enthalpy, entropy and Gibbs energy. As an example of how this can be used in future simulation efforts, the local molar Gibbs energy of a particular phase can be used as input to phase field simulations [8,51], which may be used to study the possibility of melting in severe accident scenarios [8]. Also, the specific heat capacity and enthalpy can be used in heat transfer simulations; however, the enthalpic contribution of chemical reactions to the thermal source term in nuclear fuel simulations is negligible compared to the contribution from nuclear fission and is thus not included in this work. However, this is not always the case for other multi-physics simulations pertaining to nuclear reactor operation. For example, the oxidation of Zircaloy cladding is highly exothermic; thus, chemistry plays an important role in simulating severe accident scenarios involving Zircaloy oxidation and the release of hydrogen gas.

While PWR fuel is considered in the current discussion, many other fuel types can be incorporated within this simulation framework, such as UO_2 at various ^{235}U enrichment levels (including natural uranium, as used in CANDU[4] reactors), Mixed Oxide (MOX), and advanced fuels. Isotopic evolution calculations with various components of the SCALE package have been validated with experiments involving multiple fuel types [26]. Additionally, thermodynamic models are continuing to be refined for LWR fuel and developed for advanced fuels, such as MOX, alternative oxides, carbides and nitrides [52–57]. The development of THERMOCHIMICA is continually evolving to include more representative thermodynamic models to permit convenient incorporation of new fuel models, generally based on the Compound Energy Formalism [58], and for integration into various multi-physics codes, such as BISON [10].

8. Conclusion

[4] Although CANDUs do not experience the same degree of burnup as PWRs, the increased production of fissile Pu in the rim region still significantly affects the power profile (and thus heat transfer) in the fuel [35].

The computational framework described in this paper presents a unique simulation capability that predicts high fidelity thermochemical and isotopic behavior of irradiated UO_2 fuel with application to performance and safety. The coupling of multiple physical phenomena using the AMP, ORIGEN-S and THERMOCHIMICA codes provides the capability of predicting the spatial distribution of chemical elements as a result of nuclear fission, the increased production of fissile plutonium near the rim and the resulting change in specific power (as commonly referred to as the rim effect), the formation of various phases and their composition, the oxygen-to-metal ratio, the chemical potential of every component in the system (in particular, the oxygen potential), and other related thermodynamic properties. The predicted elemental concentrations of many pertinent fission and activation products, oxygen partial pressure and oxygen-to-metal ratio agree well with measurements of highly irradiated fuel. This simulation framework provides greater insight in predicting various aspects pertaining to thermochemical behavior of nuclear fuel, such as in-reactor fuel performance, safety issues relating to defective fuel and spent fuel storage.

Acknowledgements

The authors thank V.V. Rondinella and C.T. Walker for helpful discussions regarding oxidation experiments conducted at ITU. Also, the authors thank L. Ott, I. Gauld and K. Terrani from ORNL for sharing their expertise in nuclear fuel performance and various components of the SCALE package, respectively. Finally, the authors thank all those who have contributed to the development of AMP.

The development of the Advanced Multi-Physics (AMP) nuclear fuel performance code was funded by the Fuels Integrated Performance and Safety Code (IPSC) element of the Nuclear Energy Advanced Modeling and Simulations (NEAMS) program of the U.S. Department of Energy Office of Nuclear Energy (DOE/NE), Advanced Modeling and Simulation Office (AMSO).

References

[1] D.R. Olander, Fundamental Aspects of Nuclear Reactor Fuel Elements. U.S. Department of Commerce, 1976.
[2] D. Olander, V. Mubayi, Journal of Nuclear Materials 270 (1999) 1–10.
[3] G. Berna, M. Bohn, Frapcon-1: A Computer Code for the Steady State Analysis of Oxide Fuel Rods, NUREG/CR-1463 EGG-2039, U.S. Nuclear Regulatory Commission, 1981.
[4] M. Tayal, Modelling CANDU Fuel Under Normal Operating Conditions: ELESTRES Code Description, AECL-9331, Atomic Energy of Canada Limited, 1987.
[5] K. Lassmann, Journal of Nuclear Materials 188 (1992) 295–302.
[6] J. Higgs, B. Lewis, W. Thompson, Z. He, Journal of Nuclear Materials 366 (2007) 99–128.
[7] J. Ramirez, M. Stan, P. Cristea, Journal of Nuclear Materials 359 (2006) 174–184.
[8] M. Welland, W. Thompson, B. Lewis, D. Manara, Journal of Nuclear Materials 385 (2) (2009) 358–363.
[9] B. Mihaila, M. Stan, J. Ramirez, A. Zubelewicz, P. Cristea, Journal of Nuclear Materials 394 (2009) 182–189.
[10] C. Newman, G. Hansen, D. Gaston, Journal of Nuclear Materials 392 (2009) 6–15.
[11] M. Veshchunov, V. Ozrin, V. Shestak, V. Tarasov, R. Dubourg, G. Nicaise, Nuclear Engineering and Design 236 (2006) 179–200.
[12] M. Stan, Nuclear Engineering and Technology 41 (1) (2009) 39–52.
[13] M. Amaya, J. Nakamura, F. Nagase, T. Fuketa, Journal of Nuclear Materials 414 (2011) 303–308.
[14] B. Mihaila, M. Stan, J. Crapps, D. Yun, Journal of Nuclear Materials 433 (2013) 132–142.
[15] H. Matzke, Journal of Nuclear Materials 189 (1992) 141–148.
[16] V. Rondinella, T. Wiss, Materials Today 13 (12) (2010) 24–32.
[17] H. Matzke, Nuclear Instrumentation and Methods in Physics Research B 116 (1996) 121–125.
[18] E. Corcoran, B. Lewis, W. Thompson, J. Mouris, Z. He, Journal of Nuclear Materials 414 (2010) 73–82.
[19] B. Philip, K. Clarno, W. Cochran, Software Design Document for the AMP Nuclear Fuel Performance Code, Tech. Rep. ORNL/TM-2010/34, Oak Ridge National Laboratory, 2010.
[20] The Amp Web Site. <http://www-rsicc.ornl.gov/codes/ccc/ccc7/ccc-793.html>.
[21] K. Clarno, B. Philip, W. Cochran, R. Sampath, S. Allu, P. Barai, S. Simunovic, M. Berrill, L. Ott, S. Pannala, G. Dilts, B. Mihaila, G. Yesilyurt, J. Lee, J. Banfield, Nuclear Engineering and Design 252 (2012) 108–120.
[22] K. Clarno, S. Hamilton, B. Philip, R. Sampath, S. Allu, D. Pugmire, G. Dilts, J. Banfield, T. Evans, Integrated Radiation Transport and Nuclear Fuel Performance for Assembly-level Simulations, Tech. Rep. ORNL/TM-2012/33, Oak Ridge National Laboratory, 2012.
[23] S. Allu, S. Pannala, P. Mukherjee, W. Elwasif, J. Turner, Electrochemical Society 10 (2012).
[24] Cubit Web Site. <http://cubit.sandia.gov>.
[25] G. Berna, C. Beyer, K. Davis, D. Lanning, FRAPCON-3: A Computer Code for the Calculation of Steady-state, Thermal–mechanical Behavior of Oxide Fuel Rods for High Burnup, Tech. Rep. NUREG/CR-6534, Pacific Northwest National Laboratory, 1997.
[26] I. Gauld, O. Hermann, R. Westfall, ORIGEN Scale System Module to Calculate Fuel Depletion, Actinide Transmutation, Fission Product Buildup and Decay, and Associated Radiation Terms, Tech. Rep. ORNL/TM-2005/39, Version 6, Vol. II, Sect. F7, Oak Ridge National Laboratory, 2005.
[27] S. Hamilton, K. Clarno, Transactions of the American Nuclear Society 105 (2011) 515–517.
[28] A. Schubert, P.V. Uffelen, J.V. de Laar, C. Walker, W. Haeck, Journal of Nuclear Materials 376 (2008) 1–10.
[29] K. Lassmann, C. O'Carroll, J.V. de Laar, C. Walker, Journal of Nuclear Materials 208 (1994) 223–231.
[30] M. DeHart, S. Bowman, Nuclear Technology 174 (2) (2011) 196–213.
[31] C. Walker, V. Rondinella, D. Papaioannou, S. van Winckel, W. Goll, R. Manzel, Journal of Nuclear Materials 345 (2005) 192–205.
[32] M. Piro, T. Besmann, S. Simunovic, B. Lewis, W. Thompson, Journal of Nuclear Materials 414 (3) (2011) 399–407.
[33] M. Piro, S. Simunovic, T. Besmann, B. Lewis, W. Thompson, Journal of Computational Materials Science 67 (2013) 266–272.
[34] W. Thompson, B. Lewis, E. Corcoran, M. Kaye, S. White, F. Akbari, Z. He, R. Verrall, J. Higgs, D. Thompson, T. Besmann, S. Vogel, International Journal of Materials Research 98 (10) (2007) 1004–1011.
[35] B. Lewis, W. Thompson, F. Iglesias, Comprehensive Nuclear Materials: Fission Product Chemistry in Oxide Fuels, Elsevier, 2012.
[36] H. Lukas, S. Fries, B. Sundman, Computational Thermodynamics: The Calphad Method, Cambridge University Press, 2007.
[37] J. Higgs, W. Thompson, B. Lewis, S. Vogel, Journal of Nuclear Materials 366 (2007) 297–305.
[38] H. Kleykamp, Journal of Nuclear Materials 201 (1993) 193–217.
[39] M. Kaye, B. Lewis, W. Thompson, Journal of Nuclear Materials 366 (2007) 8–27.
[40] H. Matzke, Journal of Nuclear Materials 223 (1995) 1–5.
[41] H. Kleykamp, Journal of Nuclear Materials 84 (1979) 109–117.
[42] H. Kleykamp, Journal of Nuclear Materials 80 (1988) 13–17.
[43] K. Lassmann, Nuclear Engineering and Design 57 (1980) 17–39.
[44] G. Ilas, I. Gauld, G. Radulescu, Annals of Nuclear Energy 46 (2012) 43–55.
[45] G. Ilas, I. Gauld, Analysis of Experimental Data for High Burnup PWR Spent Fuel Isotopic Validation-Vandellos II Reactor, Tech. Rep. NUREG/CR-7013, U.S. Nuclear Regulatory Commission, 2011.
[46] T. Lindemer, T. Besmann, Journal of Nuclear Materials 130 (1985) 473–488.
[47] M. Piro, Computation of Thermodynamic Equilibria Pertinent to Nuclear Materials in Multi-Physics Codes. Ph.D. Thesis, Royal Military College of Canada, 2011.
[48] V. Rondinella, Private Communication, 2012.
[49] P. Botazzoli, L. Luzzi, S. Bremier, A. Schubert, P.V. Uffelen, C. Walker, W. Haeck, W. Goll, Journal of Nuclear Materials 419 (2011) 329–338.
[50] B. Lewis, W. Thompson, M. Kleczek, K. Shaheen, M. Juhas, F. Iglesias, Journal of Nuclear Materials 408 (3) (2011) 209–223.
[51] M. Tonks, D. Gaston, P. Millett, D. Andrs, P. Talbot, Journal of Nuclear Materials 51 (2012) 20–29.
[52] C. Guéneau, N. Dupin, B. Sundman, C. Martial, J.-C. Dumas, S. Gossé, S. Chatain, F.D. Bruycker, D. Manara, R.J. Konings, Journal of Nuclear Materials 419 (1-3) (2011) 145–167.
[53] P. Chevalier, E. Fischer, B. Cheynet, Journal of Nuclear Materials 280 (2000) 136–150.
[54] P. Chevalier, E. Fischer, Journal of Nuclear Materials 288 (2001) 100–129.
[55] M. Hirota, K. Kurosaki, D. Setoyama, M. Kato, M. Osaka, T. Namekawa, M. Uno, S. Yamanaka, Journal of Nuclear Materials 344 (2005) 54–88.
[56] D. Shin, T. Besmann, Journal of Nuclear Materials 433 (2013) 227–232.
[57] T. Besmann, D. Shin, T. Lindemer, Journal of Nuclear Materials 427 (2012) 162–168.
[58] M. Hillert, Journal of Alloys and Compounds 320 (2) (2001) 161–176.